# Preparation and characterization of $Bi_{0.4}Te_{3.0}Sb_{1.6}$ nanoparticles and their thin films

M. Takashiri [a,*], S. Tanaka [b], M. Takiishi [b], M. Kihara [b], K. Miyazaki [b], H. Tsukamoto [b]

[a] *Research Division, Komatsu Ltd., 1200 Manda, Hiratsuka, Kanagawa 254-8567, Japan*

[b] *Department of Biological Functions and Engineering, Kyushu Institute of Technology, 2-4 Hibikino, Wakamatsu-ku, Kitakyushu Fukuoka 808-0196, Japan*

**Abstract**

In this article, we perform a preliminary study for assembling micro-size thermoelectric devices with low-cost fabrication by a preparation of nanoparticles and their thin films. $Bi_{0.4}Te_{3.0}Sb_{1.6}$ nanoparticles with an average size of approximately 50 nm are fabricated by a beads-milling method. The nanoparticle solution is prepared by mixing with toluene and a surfactant, and thin films with 1 μm thick are deposited on $Al_2O_3$ substrates by a printing method. The thin films are sintered at temperatures ranging from 300 to 500 $^oC$ for 60 minutes in hydrogen ambient. We investigate the thin film structures and the thermoelectric properties at room temperature. As the sintering temperature increases, hexagonal-shaped crystals are grown on the film surface while the atomic composition is almost constant throughout all the sintering temperatures. The XRD patterns indicate that all the nanoparticle thin films are found to mostly exhibit the same XRD intensities and have multiple peaks

correspond to each other. The in-plane electrical conductivity of the thin films increases but the Seebeck coefficient decreases as the sintering temperature increases. As a result, the best performance of the thermoelectric power factor of 1.3 μW/(cm $K^2$) is achieved at a sintering temperature of 350 $^oC$.

*Keywords:* nanoparticle; thin film; printing method; thermoelectric micro-device; bismuth-telluride based alloy

[a)] Author to whom correspondence should be addressed; Electronic mail:

masayuki_takashiri@komatsu.co.jp

## 1. Introduction

Thermoelectric devices for energy conversion and temperature control have been widely exploited in various industrial fields. They can be almost maintenance free, and is possible to extend the number of applications making use of thermoelectric devices by miniaturizing the devices. A typical application for the energy conversion is a wristwatch which incorporates the micro-thermoelectric device and generates electricity from the temperature difference between the surface of the body and the inside of the wristwatch [1]. The thermoelectric devices for temperature control are mainly utilized for laser diodes in order to keep their emission wavelength constant [2,3]. To further minimize the thermoelectric device size, various industrial applications might be produced, such as DNA amplification [4,5] or spot-cooling of electronic devices [6].

The primary candidate technology for miniaturizing thermoelectric devices is to apply semiconductor-processing technologies including thin film fabrication. There are presently many deposition methods to obtain thermoelectric thin films with high quality [7-11]. These thin film fabrication methods are able to produce high thermoelectric performance, but it is challenging to reduce their fabrication cost due to the waste produced in a normal etch-based process and the film thickness which is proportion to deposition time.

Printing processes such as screen and inkjet printing are attractive techniques to reduce the fabrication cost of thermoelectric devices. In this method, fine lines can be drawn on substrates directly by using solutions including thermoelectric particles so that the waste of materials can be

minimized.

There are some reports that thermoelectric films and their patterns are fabricated by the printing processes with micro-size particles [12-14]. For the further miniaturization of thermoelectric devices with fine and thin film patterns, the printing process with a nanoparticle solution is thought to be a suitable approach. This technique has been demonstrated for silicon thin film transistors (TFTs) [15]. If it can be applied to thermoelectric devices, micro-generators and micro-Peltier-coolers for micro-electronic devices might be available with low-cost fabrication.

In this study, p-type $Bi_{0.4}Te_{3.0}Sb_{1.6}$ nanoparticle thin films are investigated in terms of their structural and thermoelectric properties, as preliminary research for fabrication of the thermoelectric micro-devices. We prepare the thermoelectric material as $Bi_{0.4}Te_{3.0}Sb_{1.6}$ because the bismuth-telluride based alloys obtain high performance at room temperature [16]. The nanoparticles are fabricated by a beads-milling method, resulting in particles with an average size of approximately 50 nm. The thin films are deposited by dispersing the nanoparticles in an organic solution which is then printed onto a substrate and sintered at temperatures ranging from 300 to 500 $^{o}$C, in hydrogen ambient at atmospheric pressure. The structure of the thin films, in terms of cross-section and surface morphology, crystal orientation and atomic composition are evaluated. The thermoelectric properties, in terms of the Seebeck coefficient, the electrical conductivity and the thermoelectric power factor are determined at room temperature.

## 2. Experimental details

For the fabrication of nanoparticle p-type $Bi_{0.4}Te_{3.0}Sb_{1.6}$ thin films, we implemented three main processes. In the first step, p-type $Bi_{0.4}Te_{3.0}Sb_{1.6}$ nanoparticles were fabricated by a beads-milling method [17, 18]. As the initial material, we prepared p-type $Bi_{0.4}Te_{3.0}Sb_{1.6}$ particles with an average particle size of 20 μm by a centrifugal atomization method [7]. The total weight of the particles was 200 g. For the wet milling, 500 g of α-terpineol was used as an organic solvent. The diameter of zirconia beads was 0.2 mm, and their total weight was 500 g. The nanoparticles were fabricated by milling the mixture of the 20 μm $Bi_{0.4}Te_{3.0}Sb_{1.6}$ particles, α-terpineol, and zirconia beads for 7 hours at 3800 rpm with a "MINICER" mill (Ashizawa FineTech Inc.).

The next step was to replace the α-terpineol solvent with toluene. We fabricated nanoparticles by the beads-milling method with α-terpineol because this was an involatile solvent, which prevented oxidation of the nanoparticles due to cover of the nanoparticle-surface during the milling process. However, based on preliminary experiments we have determined that thin films deposited from a solution of nanoparticles in α-terpineol had poor adhesion onto $Al_2O_3$ substrates, whereas films deposited from a solution of nanoparticles in toluene have better adhesion. In order to remove α-terpineol from the mixture, it was heated in an electric furnace in vacuum at 150 $^{o}$C for 10 hours. Then the resulting dry nanoparticles were mixed with the toluene and a surfactant (Solsperse 39000, Avecia) whose mixing ratio by weight of the nanoparticles, toluene, and surfactant was 40 : 20 : 1.

The final processing step was to use a printing method to deposit the nanoparticle thin films onto a

substrate, which was then sintered in hydrogen. The nanoparticle solution was dropped onto the $Al_2O_3$ substrates (50 mm length, 25 mm wide and 0.5 mm thick) which were then tilted to remove the excess solution. The thickness of the thin films was approximately 1.0 μm, and the thin films had a uniform thickness across the substrate. After the printing process, the thin films were sintered to remove the toluene and the surfactant, and to melt and consolidate the nanoparticles. Samples were placed in an electric furnace that was evacuated to 1.0 Pa and purged five times with high-purity (99.999%) argon gas. Then the furnace was filled with hydrogen gas at atmospheric pressure owing to preventing the surface of nanoparticle from oxidation, and the hydrogen gas flow rate was maintained at 0.3 SLM throughout the sintering process. The sintering conditions were at temperatures ranging from 300 to 500 $^{o}$C for 60 minutes. The temperature was increased steadily at 5 K / min to the set temperature. After sintering, the samples were cooled down naturally to room temperature. The cross-section and surface morphology of $Bi_{0.4}Te_{3.0}Sb_{1.6}$ nanoparticle thin films were investigated by means of SEM, and the crystal orientation of the thin films was evaluated by XRD. The atomic composition of the thin films was examined by energy-dispersive x-ray spectroscopy (EDX).

The in-plane Seebeck coefficient of the nanoparticle thin films was measured at room temperature with an accuracy of ±5% [8]. We used two K-type thermocouples of 0.1 mm in diameter which were pressed on the center of the thin film. The distance between the thermocouples was 13 mm. One end of the thin film was connected to a heat sink and the other end to a heater. The Seebeck coefficient was determined as the ratio of the potential difference (ΔV) along the film to the temperature difference.

The in-plane electrical conductivity was also measured at room temperature by a 4-point probe method with an accuracy of ±3%. The thermoelectric power factor was estimated from the results of the Seebeck coefficient and the electrical conductivity.

**3. Results and discussion**

First, we investigate the $Bi_{0.4}Te_{3.0}Sb_{1.6}$ nanoparticles. SEM micrographs of the starting powders and nanoparticles are shown in Fig. 1. The starting powders are nearly a spherical shape, and there are many lines on the surface indicating that the powders are polycrystalline. By using the beads-milling method, it is confirmed that the $Bi_{0.4}Te_{3.0}Sb_{1.6}$ particles are sufficiently crushed, and their particle size reaches less than 200 nm. To further investigate the nanoparticles, the distribution of particle size is evaluated using a laser diffraction and scattering method (SALD-7000, Shimazu). Figure 2 shows the distribution of particle sizes, revealing that particle sizes range from 30 to 200 nm, with an average particle size of approximately 50 nm, which is 1/400th the size of the starting powders.

Secondly, the nanoparticle $Bi_{0.4}Te_{3.0}Sb_{1.6}$ thin films are printed on the $Al_2O_3$ substrates, and they are sintered in hydrogen ambient. The cross-section and surface micrographs of the thin films shown in Fig. 3 reveal the effects of sintering temperature. The thin film sintered at 300 $^{o}$C contains only nanoparticles which are essentially the same size as presented in Fig. 1 (b). At the sintering temperature of 350 $^{o}$C, crystal flakes with a hexagonal shape grow to approximately 500 nm in width and 50 nm thick on the surface of the thin film. As sintering temperatures further increase, the crystal

flakes on the surface grow larger. On the other hand, the nanoparticles existing from the substrate to the surface of the film are not grown largely when the sintering temperature increases up to 500 $^{o}$C.

The crystallization and orientation of nanoparticle $Bi_{0.4}Te_{3.0}Sb_{1.6}$ thin films are investigated by XRD (Fig. 4). The XRD peaks of $Al_2O_3$ come from the substrate. All the nanoparticle thin films sintered at temperatures ranging from 300 to 500 $^{o}$C are found mostly to exhibit the same XRD intensities and multiple peaks. This result indicates that the nanoparticles have obtained relatively good crystallinity without the sintering process, and these thin films do not have any preferred crystal orientation.

EDX provides the atomic composition of the starting powders and the resulting nanoparticle $Bi_{0.4}Te_{3.0}Sb_{1.6}$ thin films (Fig. 5). The composition of the starting powders is stoichiometric. The content of antimony is maintained constant throughout the sintering temperature. The content of bismuth is continually increased up to a sintering temperature of 400 $^{o}$C. On the other hand, the content of tellurium is decreased up to a sintering temperature of 400 $^{o}$C. However, the deviation of the atomic composition from stoichiometry is slight so it can be assumed that all sintered nanoparticle thin films in our experiment are essentially stoichiometric.

In order to investigate the impurities in the nanoparticle thin films, the EDX pattern of the thin film sintered at 500 $^{o}$C is shown in Fig. 6. The EDX pattern shows the result that the nanoparticle thin films contain carbon and oxygen as the impurities. We suggest that the carbon in the film comes from the residual material of the organic solution, and oxygen mainly comes from the $Al_2O_3$ substrate and absorption to the surface of the nanoparticles when they are exposed in the atmosphere.

The sintering temperature dependence of the thermoelectric properties of the nanoparticle $Bi_{0.4}Te_{3.0}Sb_{1.6}$ thin films, in terms of the in-plane Seebeck coefficient, the electrical conductivity and the estimated thermoelectric power factor, are shown in Fig. 7. At a sintering temperature of 300 $^{o}$C, the in-plane Seebeck coefficient and the electrical conductivity of the thin film are 258 μV/K and 1.3 S/cm, respectively. The electrical conductivity is low because the organic components such as the surfactant remain on the surface of the nanoparticles so that electrons can not pass through the surfactant layer between the nanoparticles. As the sintering temperature increases, the Seebeck coefficient of the thin films is decreased, while the electrical conductivity is increased. At a sintering temperature of 500 $^{o}$C, the in-plane Seebeck coefficient and the electrical conductivity of the thin film are 65 μV/K and 109 S/cm, respectively. Therefore, both the Seebeck coefficient and the electrical conductivity of the nanoparticle thin films can not obtain high performance at any sintering temperature. These results indicate that nanoparticle thin films obtain higher carrier concentration as the sintering temperature increases. The reason of the phenomena is not clear yet but we may consider that the residual carbon in the thin films, which separates out from the organic solution, obtains the high electrical conductivity and low Seebeck coefficient as the sintering temperature increases. Finally, the highest thermoelectric power factor achieved is 1.3 μW/(cm $K^2$) at a sintering temperature of 350 $^{o}$C. Compared to the bulk material, the thermoelectric power factor of nanoparticle thin films is still low. To further improve the thermoelectric properties of the nanoparticle thin films, it is necessary to investigate the cause of the low thermoelectric properties in detail, and optimize their processing conditions.

**4. Conclusion**

In summary, a method to fabricate $Bi_{0.4}Te_{3.0}Sb_{1.6}$ nanoparticles and their thin films is described. We use the beads-milling method to fabricate nanoparticles with an average size of approximately 50 nm. The nanoparticle solution is prepared by mixing with toluene and a surfactant, and thin films are deposited by a printing method. The thin films with approximately 1 μm thick are sintered at temperatures ranging from 300 to 500 $^{o}$C for 60 minutes in hydrogen ambient. As sintering temperatures increase, crystal flakes with a hexagonal shape grow on the surface of the thin film but the nanoparticles existing from the substrate to the surface are not largely grown. The in-plane Seebeck coefficient, electrical conductivity and the thermoelectric power factor of nanoparticle thin films are determined at room temperature. As the sintering temperature increases, the Seebeck coefficient of the thin films is decreased, while the electrical conductivity is increased. The highest thermoelectric power factor achieved is 1.3 μW/(cm $K^2$) at a sintering temperature of 350 $^{o}$C.

In this study, we reveal that the fabrication method of nanoparticles and their thin films might obtain two advantages. First, the method of the preparation of nanoparticles with average size of 50 nm and their thin films with 1 μm thick is shown that the micro-size thermoelectric generators and Peltier modules can be possible to assemble with low fabrication cost. Secondly, nanoparticle thin films might obtain low thermal conductivity from the results of their electrical conductivity. We plan to measure their thermal conductivity in the future.

**Acknowledgement**

This work is supported in part by the research program on development of innovative technology, the Japan Science and Technology Agency (JST). The authors wish to thank Prof. Dames at the University of California, Riverside, and Mr. Cannon at Kyushu Institute of Technology for the valuable comments, and the staff of the Analysis and Measurement Group at Komatsu Ltd. for technical support.

**References**

[1] M. Kishi, H. Nemoto, T. Hamao, M. Yamamoto, S. Sudou, M. Mandai, S. Yamamoto, Proceedings of 18th International Conference on Thermoelectrics, 1999, pp. 301–304.

[2] S. Murata, H. Nakada, T. Abe, H. Tanaka, A. Watabe, Jpn. J. Appl. Phys. 32 (1993) 5284-5291.

[3] M. Yamanashi, J. Appl. Phys. 80 (1996) 5494 -5502.

[4] K. Shen, X. Chen, M. Guo, J. Cheng, Sensors and Actuators B 105 (2005) 251-258.

[5] M. Yang, R. Pal, M. A. Burns, J. Micromech. Microeng. 15 (2005) 221-230.

[6] Y. Zhang, A. Shakouri, G. Zeng, Appl. Phys. Lett. 85 (2004) 2977-2979.

[7] M. Takashiri, T. Shirakawa, K. Miyazaki, H. Tsukamoto, J. Alloy. Compd. 441 (2007) 246-250.

[8] M. Takashiri, T. Borca-Tasciuc, A. Jacquot, K. Miyazaki, G. Chen, J. Appl. Phys. 100 (2006) 054315.

[9] R S. Makala, K. Jagannadham, B. C. Sales, J. Appl. Phys. 94 (2003) 3907-3918.

[10] T. C. Harman, P. J. Taylor, M. P. Walsh, B. E. LaForge, Science 297 (2002) 2229-2232.

[11] R. Venkatasubramanian, E. Siivola, T. Colpitts, B. O'Quinn, Nature 413 (2001) 597-602.

[12] T. Ohta, T. Kajikawa, Y. Kumashiro, Electrical Engineering in Japan 110 (1990) 14-23.

[13] I. Shibata, T. Nishide, J. Advanced Science 9 (1997) 183-187. [in Japanese].

[14] K. Miyazaki, T. Iida, H. Tsukamoto, Prooceedings of 22th International Conference on Thermoelectrics, 2003, pp. 641–643.

[15] T. Shimoda, Y. Matsuki, M. Furusawa, T. Aoki, I. Yudasaka, H. Tanaka, H. Iwasawa, D. Wang, M. Miyasaka, Y. Takeuchi, Nature 440 (2006) 783-786.

[16] D. M. Rowe, CRC Handbook of Thermoelectrics, CRC, London, 1995, pp. 211-256.

[17] P. Bowen, C. Carry, D. Luxembourg, and H. Hofmann, Powder Technology 157 (2005) 100-107.

[18] M. Inkyo, T. Tahara, T. Iwaki, F. Iskandar, C. Hogan Jr., and K. Okuyama, J. Colloid and Interface Science 304 (2006) 535-540.

## Figure Captions

Figure 1. SEM micrograph of $Bi_{0.4}Te_{3.0}Sb_{1.6}$ starting powders (a) and nanoparticles (b).

Figure 2. Size distribution of $Bi_{0.4}Te_{3.0}Sb_{1.6}$ nanoparticles, as determined by laser diffraction and scattering methods.

Figure 3. Cross-section and surface SEM micrographs of $Bi_{0.4}Te_{3.0}Sb_{1.6}$ nanoparticle thin films after sintering at various temperatures

Figure 4. X-ray diffraction patterns of $Bi_{0.4}Te_{3.0}Sb_{1.6}$ nanoparticle thin films after sintering at various temperatures. The peaks indicated by the open circles are detected from the $\underline{Al_2O_3}$ substrates.

Figure 5. Semi-quantitative atomic composition of $Bi_{0.4}Te_{3.0}Sb_{1.6}$ nanoparticle thin films after sintering at various temperatures, as determined by EDX. The inset table indicates the atomic composition of starting powders.

Figure 6. EDX pattern of $Bi_{0.4}Te_{3.0}Sb_{1.6}$ nanoparticle thin films after sintering at 500 $^{o}$C.

Figure 7. In-plane Seebeck coefficient, electrical conductivity and thermoelectric power factor of $Bi_{0.4}Te_{3.0}Sb_{1.6}$ nanoparticle thin films as a function of the sintering temperature.

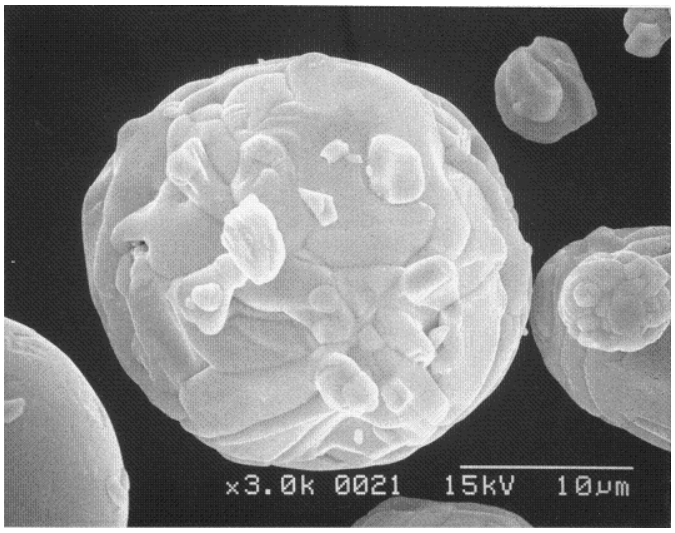


(a)

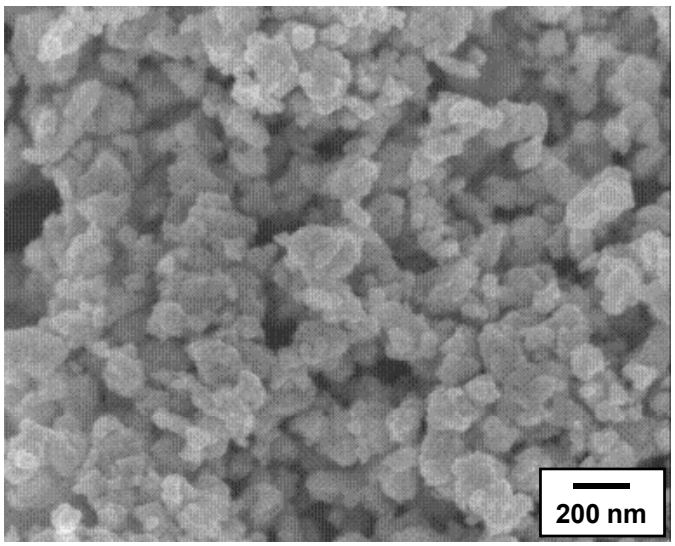


(b)

Figure 1

Figure 1. SEM micrograph of $Bi_{0.4}Te_{3.0}Sb_{1.6}$ starting powders (a) and nanoparticles (b).

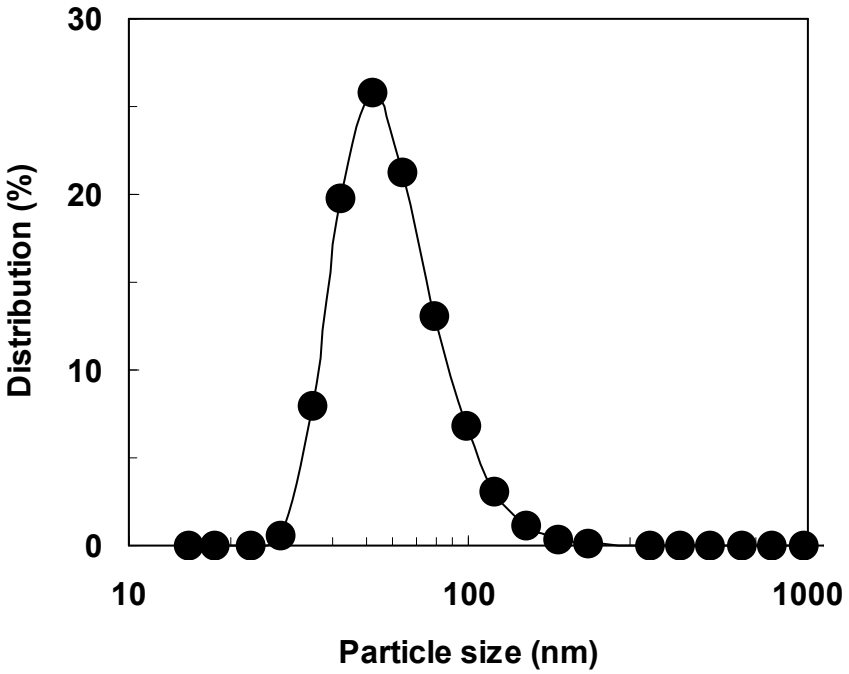


Figure 2

Figure 2. Size distribution of $Bi_{0.4}Te_{3.0}Sb_{1.6}$ nanoparticles, as determined by laser diffraction and scattering method.

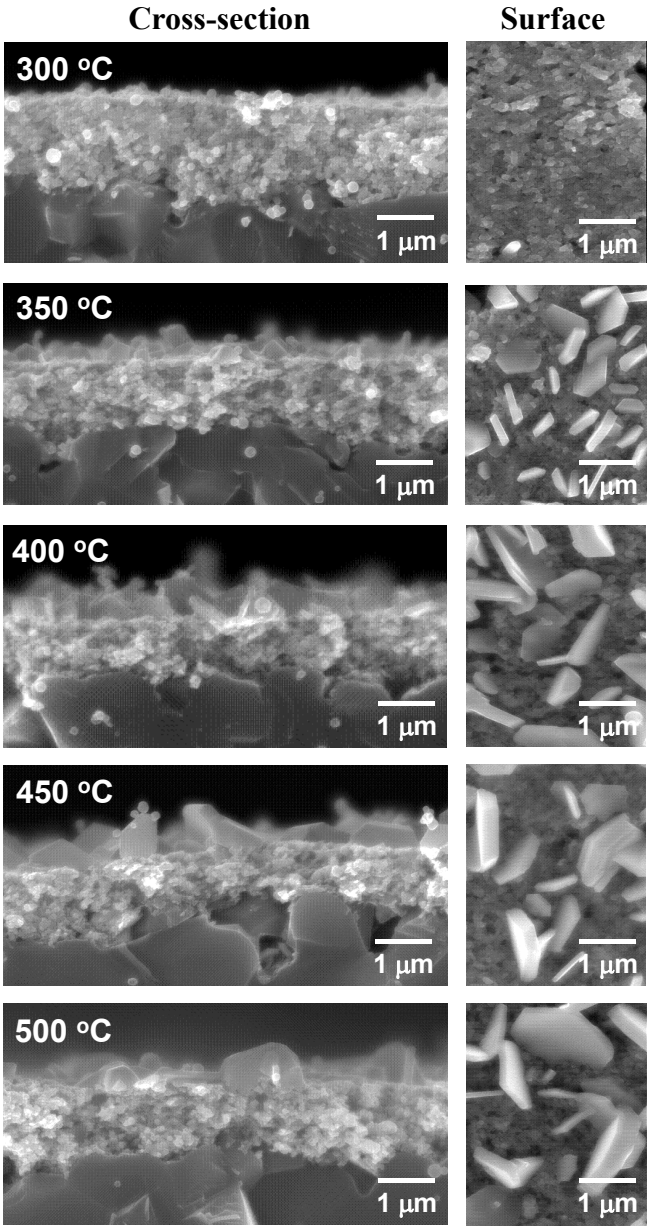


Figure 3

Figure 3. Cross-section and surface SEM micrographs of $Bi_{0.4}Te_{3.0}Sb_{1.6}$ nanoparticle thin films after sintering at various temperatures.

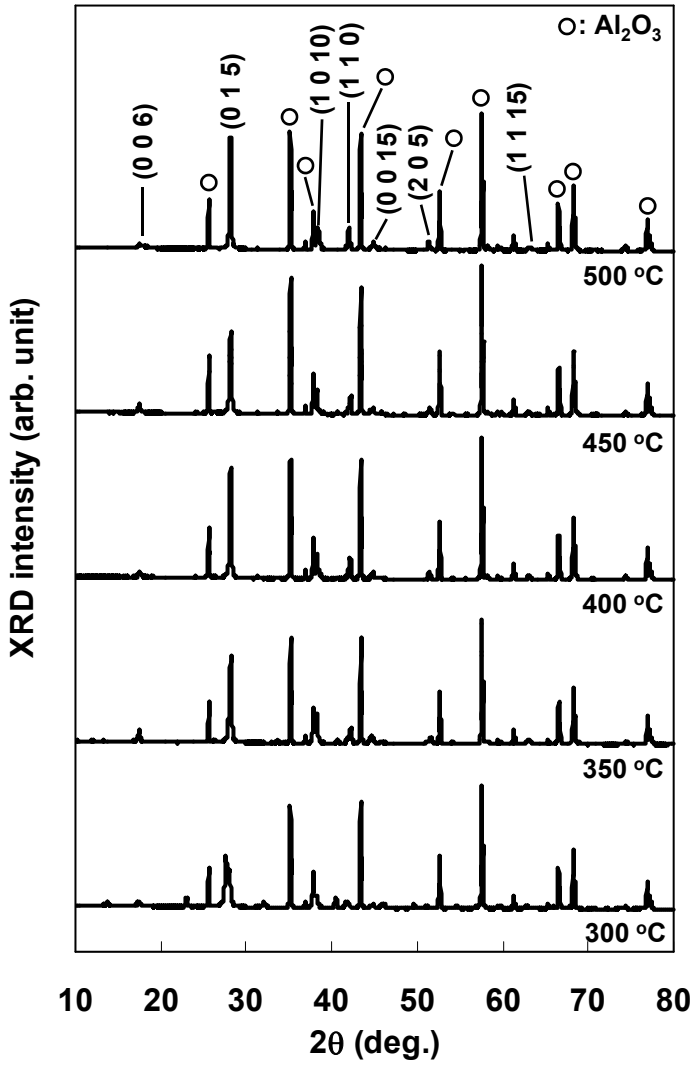


Figure 4

Figure 4. X-ray diffraction patterns of $Bi_{0.4}Te_{3.0}Sb_{1.6}$ nanoparticle thin films after sintering at various temperatures. The peaks indicated by the open circles are detected from the alumina substrates.

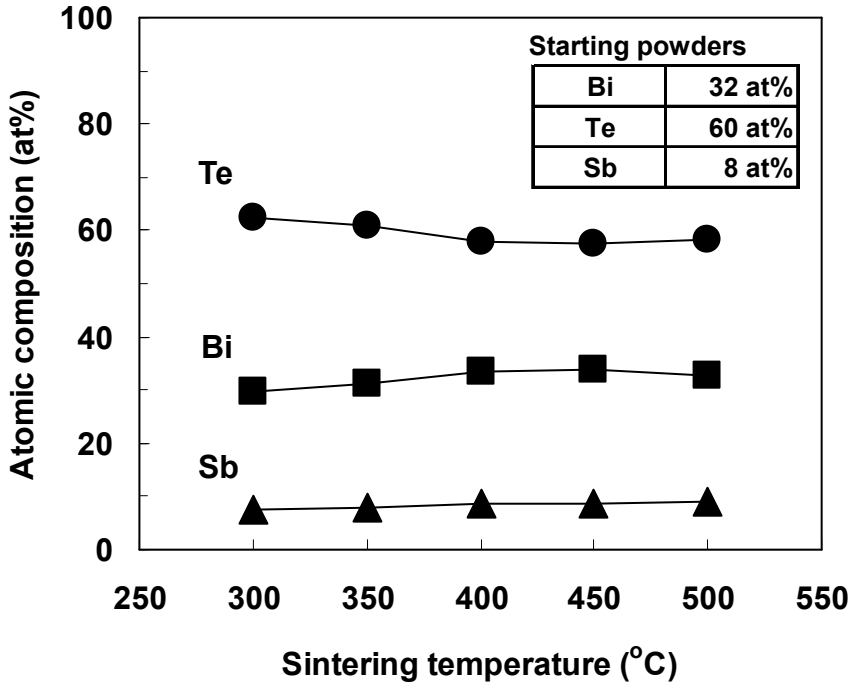


Figure 5

Figure 5. Semi-quantitative atomic composition of $Bi_{0.4}Te_{3.0}Sb_{1.6}$ nanoparticle thin films after sintering at various temperatures , as determined by EDX. The inset table indicates the atomic composition of starting powders.

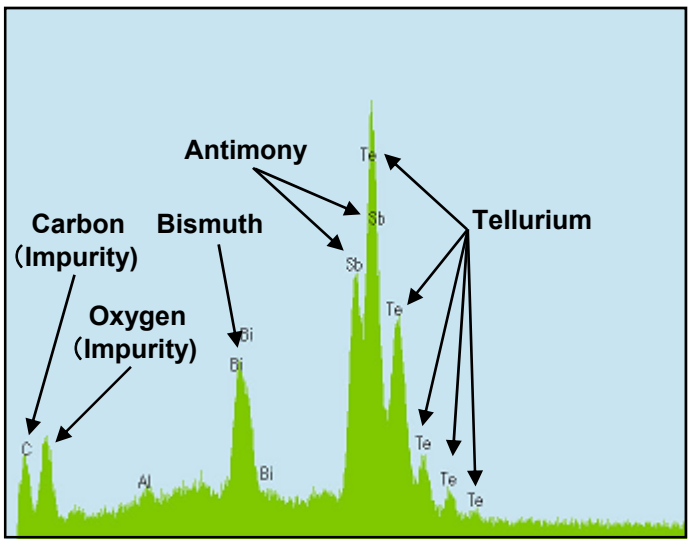


Figure 6

Figure 6. EDX pattern of $Bi_{0.4}Te_{3.0}Sb_{1.6}$ nanoparticle thin films after sintering at 500 $^{o}$C.

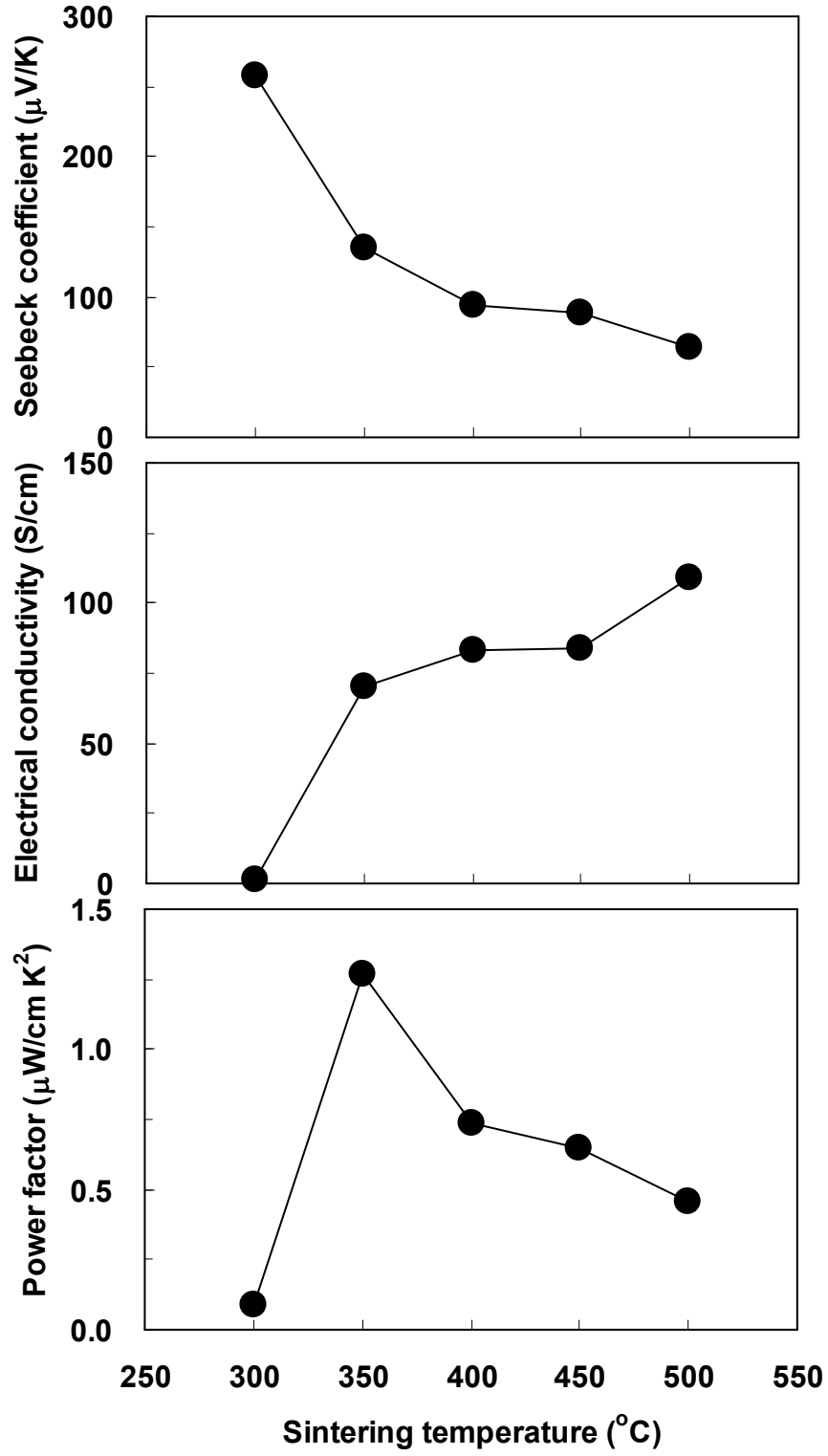


Figure 7

Figure 7. In-plane Seebeck coefficient, electrical conductivity and thermoelectric power factor of $Bi_{0.4}Te_{3.0}Sb_{1.6}$ nanoparticle thin films as a function of the sintering temperature.